Version of Record: https://journals.jps.jp/doi/10.7566/JPSJ.95.053701
Journal of the Physical Society of Japan, **95**, 053701 (2026). Manuscript Number: 18172, DOI: 10.7566/JPSJ.95.053701

First-Principles Exploration of Nd–Fe Magnetic Compounds Assisted by Transfer Learning and Genetic Algorithm

Sayaka Ito[1], Insung Seo[2], Shimpei Tanaka[3], Mitsuru Endo[4], Yukio Tsutsui[5], Tomonori Tanaka[1], and Yoshihiro Gohda[1]*

[1]*Department of Materials Science and Engineering, Institute of Science Tokyo, Yokohama 226-8501, Japan*
[2]*Graduate School of Natural Science and Technology, Shimane University, Matsue 690-8504, Japan*
[3]*Tsukuba Research Laboratory, Corporate Technology Division, YASKAWA Electric Corporation, Tsukuba 300-2635, Japan*
[4]*Department of Mechanical Engineering, Institute of Science Tokyo, Tokyo 152-8550, Japan*
[5]*Department of Electrical and Electronic Engineering, Institute of Science Tokyo, Tokyo 152-8550, Japan*

We propose a scheme to accelerate the screening of magnetic compounds with high magnetization and low formation energy by integrating transfer-learned machine learning models with a genetic algorithm. Applying this framework to the Nd–Fe binary system, we identify multiple compounds absent from existing databases. The transfer learning on density functional theory data significantly improves formation energy prediction accuracy. Notably, a discovered cubic $NdFe_{15}$ structure exhibits both high saturation magnetization and relatively low formation energy.

High-performance permanent magnets are indispensable for motors in industrial robots and electric vehicles, which require miniaturization and mass reduction.[1)] Since the discovery of neodymium magnets (main phase: $Nd_2Fe_{14}B$) by Sagawa et al. in 1984,[2)] extensive efforts have been made to improve their magnetic properties.[3–8)] The performance of these magnets has also been examined from many aspects using first-principles calculations.[9–16)] To overcome the limits of existing permanent magnets, finding novel compounds with superior properties is imperative. To this end, materials exploration utilizing machine learning, which has been widely applied across various material systems, has emerged as a highly promising approach.[17)] Furthermore, the rapid development of machine learning potentials has made it possible to rapidly obtain stable structures.[18–20)] Therefore, combining crystal structure prediction methods—implemented in such as CrySPY,[21)] AIRSS,[22)] and CALYPSO[23)]—with machine learning-based potentials and stability evaluation schemes would enable the high-throughput screening of candidate materials for permanent magnets.[24,25)] In this letter, we demonstrate a scheme integrating a genetic algorithm with a graph neural network (GNN) potential, specifically optimized for the Nd–Fe binary system via transfer learning. We applied this framework to search for high-magnetization phases that do not exist in current databases. Our approach couples the Universal Structure Predictor: Evolutionary Xtallography (USPEX) code[26)] with the Atomistic Line Graph Neural Network (ALIGNN),[27,28)] utilizing the software implementation provided by NIST.[29)] USPEX generates candidate crystal structures using genetic operations, while ALIGNN serves as a surrogate model to rapidly evaluate formation energies. Although pre-trained GNN models on the JARVIS-DFT[30)] or Materials Project[31)] databases exhibit high generalizability, they often lack the precision required for specific magnetic systems. To address this challenge, we employed transfer learning.

We constructed a training dataset by performing DFT calculations on arbitrary binary structures derived from the Materials Project with a composition ratio of 1:5 or higher (Fe-rich), substituting the constituent elements with Nd and Fe. The DFT calculations were performed using the Vienna Ab initio Simulation Package[32,33)] based on the Hohenberg–Kohn–Sham theory.[34,35)] We used the projector augmented-wave method,[36)] and the exchange-correlation interaction was treated within the generalized gradient approximation parameterized by Perdew, Burke, and Ernzerhof.[37)] The plane-wave cutoff energy was set to 350 eV. To optimize the ALIGNN models for the Nd–Fe system using a limited dataset (104 structures), we fine-tuned only the output-fully-connected layer to minimize the loss function for the target properties (formation energy and magnetic moment), while keeping the weights of the input and intermediate layers frozen. This approach allows for efficient domain adaptation while minimizing the risk of overfitting. In this learning process, we adopted a strategy of freezing the graph convolutional layers and training only the output layer. It is inferred that this allowed for the efficient correction of formation energy and magnetic moments in the Nd–Fe system while retaining the universal geometric features of crystal structures learned from large-scale data, leading to an improvement in predictive accuracy. The efficacy of this transfer learning method was quantitatively validated. We utilized three specific ALIGNN models pre-trained on the JARVIS-DFT dataset as starting points: the regression models for formation energy and total magnetic moment, and the force field model (ALIGNN-FF) for total energy and atomic forces. While various foundation models have been developed recently, ALIGNN was selected for two primary reasons essential to this study. First, its architecture, based on line graphs, explicitly encodes bond angular information (three-body interactions), providing a superior description of local atomic environments compared to standard graph neural networks. This capability is crucial for accurately distinguishing the energetics of complex Nd–Fe polymorphs. Second, ALIGNN-FF has been explicitly demonstrated to function effectively as an evaluation function

*E-mail: gohda@mct.isct.ac.jp

for genetic algorithms (GA) in previous literature,[28] ensuring its compatibility and reliability for our structure search workflow. Figure 1 presents the parity plots for the regression models. In the evaluation of the prediction accuracy for both formation energy and magnetic moment, the train-test split was set to 80:20. Regarding the formation energy [Fig.1(a)], the coefficient of determination (R^2) improved from 0.47 to 0.93, enabling reliable structure screening. Furthermore, the regression model for magnetic moment prediction [Fig. 1(b)] demonstrated a substantial reduction in the mean absolute error (MAE), decreasing from 6.53 to 0.109 μ_B per atom. The coefficient of determination (R^2) for the magnetic moment prediction improved significantly from −332.6940 (pre-trained model) to 0.8099 (transfer-learned model). This remarkable improvement highlights the effectiveness of transfer learning, particularly because rare-earth magnetic materials accounted for only 0.4% of the original pre-trained dataset. In addition, the force field model used for structural optimization was also transfer-learned using 5-fold cross-validation[38] with an 80:20 train-test split.

Using the transfer-learned ALIGNN model, we conducted an extensive genetic structure search over the Nd–Fe binary composition range ($6 \leq N \leq 100$ atoms). In this study, ALIGNN-FF[28] was employed for structural relaxation at each step of the genetic algorithm, while ALIGNN[27] was used for fitness evaluation. These machine learning models were specialized for the Nd–Fe system via transfer learning. Although ALIGNN-FF is less accurate than DFT, its computational speed is several orders of magnitude faster, enabling the low-cost optimization and stability evaluation of the massive number of candidate structures generated by the GA. The evolutionary search proceeded as follows: First, an initial population was generated from structures with Nd and Fe arranged in random space groups and topologies.[39] Next, structural optimization predictions were performed for each individual using ALIGNN-FF. Subsequently, the fitness of each individual was evaluated based on Pareto optimization[40] for low formation energy and high magnetic moment predicted by ALIGNN. The next generation of structures was then produced through genetic operations such as crossover and mutation.[39,41,42] This process repeated until the best structure remained unchanged for a certain number of generations, at which point it was considered the optimal solution. Structures with low predicted formation energies were selected for final high-precision DFT relaxation. We focused on identifying Fe-rich phases with saturation magnetization exceeding that of $Nd_2Fe_{14}B$ (1.89 T). Although $Nd_2Fe_{14}B$ provides the ultimate benchmark, our structure searches are restricted to Nd–Fe binary phases; we therefore adopt the saturation magnetization of $Nd_2Fe_{14}B_0$ (1.99 T)—the fully relaxed structure obtained after removing B from $Nd_2Fe_{14}B$—as a practical reference. The crystal structure of $Nd_2Fe_{14}B_0$ is shown in Fig. 2.

Figure 3 shows the distribution of saturation magnetization M_s versus formation energy for the discovered structures. We focused on exploring Nd–Fe systems with M_s exceeding 1.99 T, which corresponds to the magnetization of $Nd_2Fe_{14}B_0$. A quantitative analysis of the thermodynamic scale of metastability has revealed that many synthesizable inorganic crystals exhibit low but still positive formation energies.[43] As shown in the figure, several structures were identified that possess both relatively low (albeit positive) formation energy

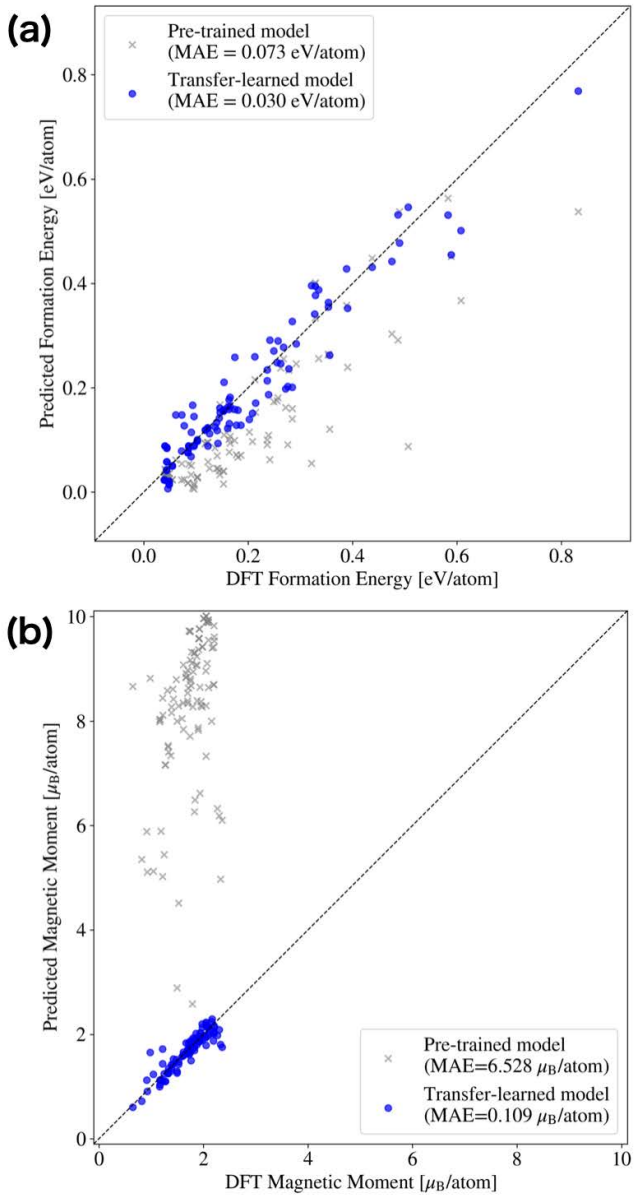

Fig. 1. (Color online) Parity plots comparing DFT-calculated values and ALIGNN predictions for the Nd–Fe system after transfer learning: (a) formation energy and (b) magnetic moment per atom. The diagonal lines indicate perfect agreement.

and high magnetization, locating them in the promising region of the map. It is known that binary Nd–Fe intermetallic compounds are generally metastable compared to the phase separation into Fe and Nd-rich phases.[44] Our results are consistent with this trend. However, this study was conducted based on the premise of expanding these binary compounds into ternary systems via the insertion of light elements to potentially achieve negative formation energies, a concept already demonstrated in our previous studies.[45,46] Therefore, while all the discovered high-magnetization structures exhibit positive formation energies as binary phases, they were researched as promising precursors for stabilization through third-element doping.

Among the promising candidates, a cubic compound with the composition $NdFe_{15}$ was identified. Figure 4 shows its crystal structure. Based on the atomic ratio (Nd:1, Fe:15) and space group ($Pm\bar{3}m$, No. 221), this system corresponds to a

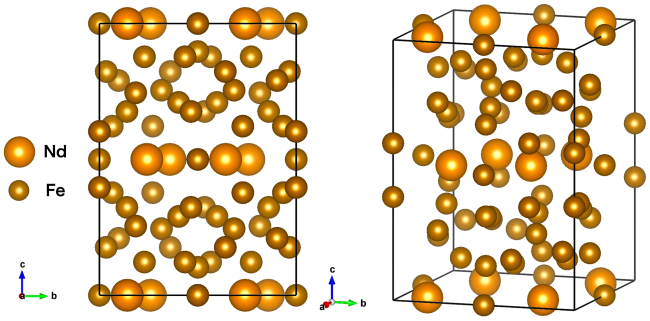

Fig. 2. (Color online) Crystal structure of the reference $Nd_2Fe_{14}B_0$. Large spheres represent Nd atoms, and small spheres represent Fe atoms.

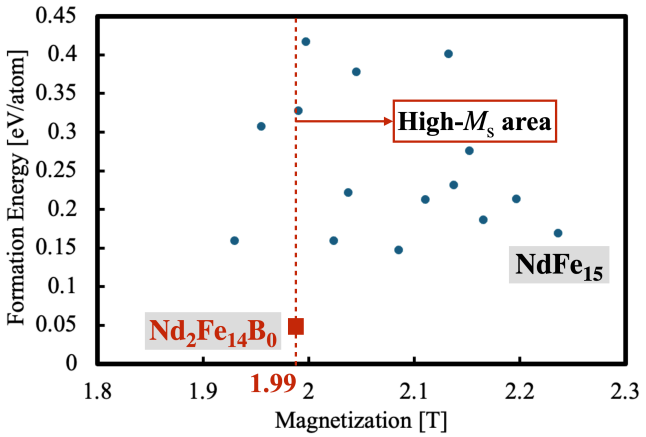

Fig. 3. (Color online) Formation energy and saturation magnetization for the Nd–Fe binary structures obtained from the evolutionary search (circles). The square indicates the reference $Nd_2Fe_{14}B_0$. Several candidates exhibit superior magnetization exceeding the reference value.

$2 \times 2 \times 2$ supercell of bcc Fe (total 16 atoms), where one corner atom is substituted by Nd. In the DFT calculations, we adopted the open-core approximation (frozen-core approximation), treating the Nd $4f$ electrons as fixed core electron clouds. Consequently, the saturation magnetization M_s was calculated by summing the spin magnetic moments of valence electrons obtained from DFT calculations $\sum m_{\mathrm{spin}}$ and the localized magnetic moment of the rare-earth $4f$ electrons

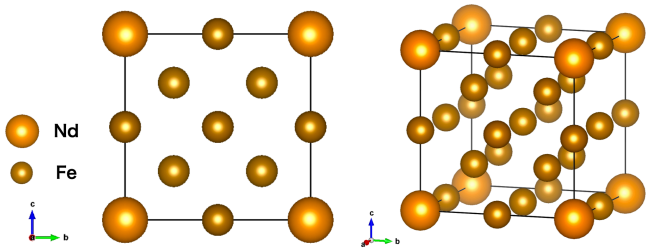

Fig. 4. (Color online) VESTA[47] visualization of the crystal structure for the discovered cubic $NdFe_{15}$ with a lattice constant of 5.85 Å. Large spheres represent Nd atoms, and small spheres represent Fe atoms. This structure exhibits the highest saturation magnetization among the discovered structures.

Table I. Calculated magnetic moments for the $NdFe_{15}$ structure. The magnetic moment of Nd includes $m_{\mathrm{RE}4f}$.

Space group	Lattice parameter (Å)	
$Pm\bar{3}m$ (No. 221)	$a = b = c = 5.852$	
Element	Wyckoff position	Magnetic moment (μ_B)
Nd	1a	2.97
Fe	1b	2.25
Fe	3c	2.43
Fe	3d	2.44
Fe	8g	2.34
Total		**38.54**

$m_{\mathrm{RE}4f}$:

$$M_s = \frac{1}{V}\left[\sum m_{\mathrm{spin}} + n_{\mathrm{RE}} m_{\mathrm{RE}4f}\right], \tag{1}$$

where V is the unit cell volume and n_{RE} is the number of Nd atoms in the unit cell. For Nd^{3+} ($4f^3$), $m_{\mathrm{RE}4f}$ is derived from the Russell–Saunders coupling scheme using the total angular momentum quantum number $J = 9/2$ and Landé g-factor $g_J = 8/11$:

$$m_{\mathrm{Nd}4f} = g_J J \mu_B \approx 3.273\,\mu_B. \tag{2}$$

This $NdFe_{15}$ phase exhibits a high saturation magnetization of approximately 2.24 T, which is competitive with existing high-performance magnet materials. The high magnetization can be attributed to the enhancement of Fe moments. While the magnetic moment of pure bcc Fe is approximately 2.2 μ_B, the site-specific magnetic moments of $NdFe_{15}$ (Table I) indicate that the moments at 3c, 3d, and 8g sites are significantly enhanced, ranging from 2.34 to 2.43 μ_B. While the cubic symmetry implies isotropic magnetic properties, its high magnetization and relatively low formation energy make it an interesting precursor for further material design.

We also evaluated the Heisenberg exchange coupling parameters J_{ij} of $NdFe_{15}$ using the AkaiKKR package,[48] based on DFT and the Green's function method, as shown in Fig. 5. Here, the Heisenberg model is defined as

$$E = -\sum_{i \neq j} J_{ij}\, \hat{\mathbf{e}}_i \cdot \hat{\mathbf{e}}_j, \tag{3}$$

where $\hat{\mathbf{e}}_i$ is the unit vector specifying the spin direction at site i. The sum $\sum_{i \neq j}$ runs over all pairs with $i \neq j$ (self-terms are excluded), so that each pair is counted twice. For reference, the results for bcc Fe are also shown. As also shown in Fig. 5, the Curie temperature within the mean-field approximation, T_C^{MFA}, is higher than that of bcc Fe, reflecting the larger overall exchange scale entering the mean-field sum over J_{ij}. This trend is favorable from the viewpoint of magnetic applications requiring higher transition temperatures.

In addition to the cubic phase, our search also detected other high-magnetization Nd–Fe binary compounds with tetragonal and hexagonal symmetries. Although the discovered binary phases possess positive formation energies, the incorporation of interstitial light elements (such as B, C, N, O, and F) offers a promising route for stabilization. It has been demonstrated in previous first-principles studies and experimental reports that interstitial doping can significantly

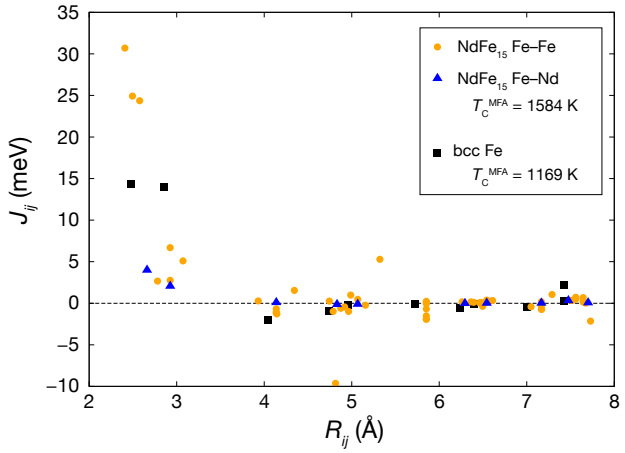

Fig. 5. (Color online) Exchange coupling parameters J_{ij} as a function of the interatomic distance R_{ij}. Squares denote the results for bcc Fe, whereas circles and triangles denote the Fe–Fe and Fe–Nd pairs in $NdFe_{15}$, respectively. Curie temperatures within the mean-field approximation, T_C^{MFA}, are also shown.

reduce the formation energy of Nd–Fe compounds, potentially shifting it from positive to negative values, thereby thermodynamically stabilizing the structure.[45,46,49,50] Inspired by these findings, future work will focus on stabilizing the high-magnetization structures discovered here by exploring the interstitial solid solution of these light elements. Furthermore, we anticipate that such incorporation of interstitial light elements could induce a distortion in the cubic $NdFe_{15}$ host, transforming its isotropic lattice into an anisotropic one, analogous to the transformation from cubic bcc Fe to body-centered tetragonal α''-$Fe_{16}N_2$ upon nitrogen insertion.[51] In future work, we will extend the framework by incorporating magnetocrystalline anisotropy into the genetic-algorithm fitness function to enable more efficient exploration of permanent-magnet compounds.

Acknowledgment This work was partly supported by MEXT-DXMag (Grant No. JPMXP1122715503), JSPS-KAKENHI (Grant No. JP24K01144). The calculations were partly carried out by using supercomputers at ISSP, The University of Tokyo, and TSUBAME4.0, Institute of Science Tokyo.

1) J. M. D. Coey, Engineering **6**, 119 (2020).
2) M. Sagawa, S. Fujimura, N. Togawa, H. Yamamoto, and Y. Matsuura, J. Appl. Phys. **55**, 2083 (1984).
3) J. F. Herbst, Rev. Mod. Phys. **63**, 819 (1991).
4) S. Hirosawa, M. Nishino, and S. Miyashita, Adv. Nat. Sci: Nanosci. Nanotechnol. **8**, 013002 (2017).
5) H. Sepehri-Amin, T. Ohkubo, T. Shima, and K. Hono, Acta Mater. **60**, 819 (2012).
6) H. Sepehri-Amin, T. Ohkubo, and K. Hono, Acta Mater. **61**, 1982 (2013).
7) T. T. Sasaki, T. Ohkubo, and K. Hono, Acta Mater. **115**, 269 (2016).
8) W. F. Li, T. Ohkubo, K. Hono, and M. Sagawa, J. Magn. Magn. Mater. **321**, 1100 (2009).
9) Y. Gohda, Y. Tatetsu, and S. Tsuneyuki, Mater. Trans. **59**, 332 (2018).
10) Y. Gohda, Sci. Technol. Adv. Mater. **22**, 113 (2021).
11) H. Okumura, T. Fukushima, H. Akai, and M. Ogura, Solid State Commun. **373-374**, 115257 (2023).
12) H. Akai, Scr. Mater. **154**, 300 (2018).
13) S. Miyashita, M. Nishino, Y. Toga, T. Hinokihara, I. E. Uysal, T. Miyake, H. Akai, S. Hirosawa, and A. Sakuma, Sci. Technol. Adv. Mater. **22**, 658 (2021).
14) M. Ogura A. Mashiyama, and H. Akai, J. Phys. Soc. Jpn. **84**, 084702 (2015).
15) T. Miyake, K. Terakura, Y. Harashima, H. Kino, and S. Ishibashi, J. Phys. Soc. Jpn. **83**, 043702 (2014).
16) Y. Harashima, K. Terakura, H. Kino, S. Ishibashi, and T. Miyake, Phys. Rev. B **92**, 184426 (2016).
17) A. Merchant, S. Batzner, S. S. Schoenholz, M. Aykol, G. Cheon, and E. D. Cubuk, Nature **624**, 80 (2023).
18) T. Xie and J. C. Grossman, Phys. Rev. Lett. **120**, 145301 (2018).
19) C. Chen, W. Ye, Y. Zuo, C. Zheng, and S. P. Ong, Chem. Mater. **31**, 3564 (2019).
20) B. Deng, P. Zhong, K. Jun, J. Riebesell, K. Han, C. J. Bartel, and G. Ceder, Nat. Mach. Intell. **5**, 1031 (2023).
21) T. Yamashita, H. Kanehira, N. Sato, H. Kino, H. Sawa, and T. Oguchi, Sci. Technol. Adv. Mater.: Methods **1**, 87 (2021).
22) C. J. Pickard and R. J. Needs, J. Phys.: Condens. Matter **23**, 053201 (2011).
23) Y. Wang, J. Lv, L. Zhu, and Y. Ma, Phys. Rev. B **82**, 094116 (2010).
24) T. Miyake, Y. Harashima, T. Fukazawa, and H. Akai, Sci. Technol. Adv. Mater. **22**, 543 (2021).
25) T. Miyake, JSAP Rev. **2023**, 230205 (2023).
26) A. R. Oganov and C. W. Glass, J. Chem. Phys. **124**, 244704 (2006).
27) K. Choudhary and B. DeCost, npj Comput. Mater. **7**, 185 (2021).
28) K. Choudhary, B. DeCost, L. Major, K. Butler, J. Thiyagalingam, and F. Tavazza, Digital Discovery **2**, 346 (2023).
29) K. Choudhary and B. DeCost, *ALIGNN: Atomistic Line Graph Neural Network* (National Institute of Standards and Technology, 2024) https://doi.org/10.18434/mds2-3170.
30) K. Choudhary, K. F. Garrity, A. C. E. Reid, B. DeCost, A. J. Biacchi, A. R. Hight Walker, Z. Trautt, J. Hattrick-Simpers, A. G. Kusne, A. Centrone, A. Davydov, J. Jiang, R. Pachter, G. Cheon, E. Reed, A. Agrawal, X. Qian, V. Sharma, H. Zhuang, S. V. Kalinin, B. G. Sumpter, G. Pilania, P. Acar, S. Mandal, K. Haule, D. Vanderbilt, K. Rabe, and F. Tavazza, npj Comput. Mater. **6**, 173 (2020).
31) A. Jain, S. P. Ong, G. Hautier, W. Chen, W. D. Richards, S. Dacek, S. Cholia, D. Gunter, D. Skinner, G. Ceder, and K. A. Persson, APL Mater. **1**, 011002 (2013).
32) G. Kresse and J. Furthmüller, Phys. Rev. B **54**, 11169 (1996).
33) G. Kresse and D. Joubert, Phys. Rev. B **59**, 1758 (1999).
34) P. Hohenberg and W. Kohn, Phys. Rev. **136**, B864 (1964).
35) W. Kohn and L. J. Sham, Phys. Rev. **140**, A1133 (1965).
36) P. E. Blöchl, Phys. Rev. B **50**, 17953 (1994).
37) J. P. Perdew, K. Burke, and M. Ernzerhof, Phys. Rev. Lett. **77**, 3865 (1996).
38) M. Stone, J. R. Stat. Soc. B **36**, 111 (1974).
39) C. W. Glass, A. R. Oganov, and N. Hansen, Comput. Phys. Commun. **175**, 713 (2006).
40) K. Deb, A. Pratap, S. Agarwal, and T. Meyarivan, IEEE Trans. Evol. Comput. **6**, 182 (2002).
41) A. R. Oganov, A. O. Lyakhov, and M. Valle, Acc. Chem. Res. **44**, 227 (2011).
42) A. O. Lyakhov, A. R. Oganov, H. T. Stokes, and Q. Zhu, Comput. Phys. Commun. **184**, 1172 (2013).
43) W. Sun, S. T. Dacek, S. P. Ong, G. Hautier, A. Jain, W. D. Richards, A. C. Gamst, K. A. Persson, and G. Ceder, Sci. Adv. **2**, e1600225 (2016).
44) K. H. J. Buschow, Rep. Prog. Phys. **40**, 1179 (1977).
45) Y. Tatetsu, Y. Harashima, T. Miyake, and Y. Gohda, Phys. Rev. Materials **2**, 074410 (2018).
46) I. Seo, S. Tanaka, M. Endo, and Y. Gohda, Appl. Phys. Express **17**, 075502 (2024).
47) K. Momma and F. Izumi, J. Appl. Crystallogr. **44**, 1272 (2011).
48) H. Akai, J. Phys.:Condens. Matter **1**, 8045–8064 (1989).
49) Y. Hirayama, Y. K. Takahashi, S. Hirosawa, and K. Hono, Scr. Mater. **95**, 70 (2015).
50) Y. Hirayama, Y. K. Takahashi, S. Hirosawa, and K. Hono, Scr. Mater. **138**, 62 (2017).
51) H. Sims, W. H. Butler, M. Richter, K. Koepernik, E. Şaşıoğlu, C. Friedrich, and S. Blügel, Phys. Rev. B **86**, 174422 (2012).